Ultrasonics - Sonochemistry 48 (2018) 299–310

Contents lists available at ScienceDirect

Ultrasonics - Sonochemistry

journal homepage: www.elsevier.com/locate/ultson

Development of LTA zeolite membrane from clay by sonication assisted method at room temperature for H_2-CO_2 and CO_2-CH_4 separation

Mitali Sen[a], Kausik Dana[b], Nandini Das[a,*]

[a] Ceramic Membrane Division, CSIR-Central Glass & Ceramic Research Institute, Kolkata 700 032, India
[b] Clay and Traditional Ceramics Division, CSIR-Central Glass & Ceramic Research Institute, Kolkata 700 032, India

ARTICLE INFO

Keywords:
Sonication
Montmorillonite clay
Zeolite
Membrane
Gas separation

ABSTRACT

In this work, sodium aluminosilicate zeolite powder and membranes were synthesized by ultrasonic irradiation at room temperature using montmorillonite clay as precursor material. For comparison, same zeolite powder and membranes were synthesized at 100 °C also. The synthesized zeolites were characterized by X-ray diffraction (XRD), infrared (IR) spectral analysis, and field-emission scanning electron microscopy (FESEM). XRD and IR results showed that phase pure mainly LTA phase was formed after 15 days of aging at room temperature. By using the zeolite powders as seeds, membranes were synthesized on clay alumina support tubes at room temperature and also at 100 °C. In both the cases membranes were formed on support surface. The membrane thickness was found to be 15 μm. The performances of the membranes were evaluated by single gas as well as mixture gas permeation measurement for H_2-CO_2 and CO_2-CH_4 respectively. The H_2–CO_2 and CO_2-CH_4 separation selectivity for the mixture gas of the membrane was found to 16.2 and 20.9 at room temperature respectively. To the best of our knowledge, there is no report of synthesis of zeolite membrane at room temperature using clay as raw materials. For the first time we have reported the synthesis of alumino-silicate zeolite membrane on clay alumina support surface using clay as starting material by sonochemical method at room temperature.

1. Introduction

The increasing demand for "clean" and efficient energy has resulted in an increased global willingness to embrace the proposed "hydrogen economy" as a potential long term solution to the growing energy crisis. Hydrogen has been considered as next generation clean fuel. But it is not available in pure form in nature [1]. Usually hydrogen can be produced from SMR (steam methane reforming) process which consists primarily of the highly endothermic SMR reaction ($CH_4 + H_2O \rightarrow CO + 3H_2$) followed by the Water Gas Shift reaction (WGS) ($CO + H_2O \rightarrow CO_2 + H_2$) [2]. Ultimately, a mixture of H_2, CO_2, and CH_4 is formed. Consequently H_2 should be removed from the reaction mixture, mainly from CO_2 to increase the ultimate efficiency of the process. Currently H_2 can be purified by pressure swing adsorption (PSA) [3,4], fractional/cryogenic distillation [5,6], membrane based separation process [7,8] etc. Membranes can be an alternative to energy demanding separation processes such as distillation and absorption and can enhance conversion of equilibrium limited reactions. Inorganic microporous membranes are most promising material for high temperature H_2 separation because of their high thermal and chemical stabilities. Dense Pd membrane and silica membranes are currently used for separation of H_2, CO_2 and other gases [9,10]. Among all inorganic materials Zeolites are considered as potential material for gas separation applications due to their advantages of well-defined pore structure, adsorption properties, high thermal and chemical stability [11,12]. In general, zeolites are microporous crystalline alumino-silicates, with exchangeable cation. It shows cage-like structures of precise geometry with pores of uniform shape [13].

Zeolites are typically synthesized from a gel under hydrothermal condition with alkali metal cation or organic amine etc as structure directing agent (SDA). However, main disadvantage of existing methods of zeolite synthesis lies on high raw material cost and high temperature synthesis method like hydrothermal etc. which are more or less far apart from the principles of green chemistry.

This hydrothermal synthesis of zeolite is not in environmentally friendly and energy saving process. Traditionally in green chemistry, the synthesis processes has been chosen so that it reduces or eliminates the use or generation of hazardous substance in the design manufacture and application of chemical products. It emphatic the economy of the resource and energy, minimizing waste and cost, reducing chemical hazard and ensuing process safety [14].

Currently, attention has been paid to use green chemistry in

* Corresponding author at: Ceramic Membrane Division, Central Glass and Ceramic Research Institute, CSIR, 196, Raja SC Mullick Road, Jadavpur, Kolkata 700 032, India.
E-mail address: dasnandini@cgcri.res.in (N. Das).

https://doi.org/10.1016/j.ultsonch.2018.06.007
Received 15 March 2018; Received in revised form 18 May 2018; Accepted 13 June 2018

synthesis by using environmental friendly resources and has become one of the main objects of this work. The hydrothermal synthesis method is usually conducted at high temperature and high pressure, which make the process expensive, with increasing energy consumption. So efforts have been made for green synthesis of zeolite materials.

Further, the production of zeolites from alternative sources of silica and alumina such as volcanic glasses [15] fly ash [16], rice husk [17] and clays [18] continue to be investigated. Several investigators have studied the preparation of zeolite from kaolin (clay) and have been successful in the synthesis of zeolites, mainly zeolite A [19], NaA [20], faujasites [21] and NaP [22]. Clay materials which are the most abundant materials in the earth have many interesting properties like low cost, high sorption, ion exchange and good adsorbent.

So, in this work efforts have been made for green synthesis of alumino-silicate zeolite materials for membrane preparation from low cost material bentonite (montmorillonite) clay. Sonochemical method is a green and feasible technique. High power ultrasound produces strong cavitation in aqueous solution causing shock wave and reactive free radicals (e.g., ·OH, HO_2·, and O·) by the violent collapse of the cavitation bubble [23]. In sonochemical method, application of ultrasound to chemical reactions influences the physicochemical phenomena related to nucleation and crystal growth, occurring during crystallization which substantially reduce the crystallization time at room temperature compared to conventional chemical methods [24]. In this work we have proposed to synthesize LTA zeolite membrane for CO_2 separation from clay material and synthesized by green method i.e. sonochemical method at room temperature. Here, a simple sonochemical route was designed to prepare zeolite membrane in which bentonite (Montmorillonite (Mt)) clay and NaOH used as the main source of silicon and aluminum, improving crystallization time and temperature for lower values.

2. Experimental

2.1. Materials

Bentonite clay used in this study was of Indian origin Neelkanth Minechem, India. Other chemicals used for this synthesis was sodium hydroxide pellets (Merck, India), decaline (Merck, India), hydrogen peroxide (Merck, India), Poly-diallyldimethylammonium chloride solution (Poly-DADMAC, 20% in water) (Sigma Aldrich), acetone (Merck, India), and distilled water.

2.2. Purification of clay

Before using the bentonite clay, suspension was made with clay and deionized water to remove impurities. Particles less than 1 μm were separated from clay slurry by homogeneous dispersion followed by gravity separation. The submicron fraction of the clay separated by sedimentation was analyzed for particle size by dynamic light scattering technique and found to be Montmorillonite (Mt) by XRD and electron microscopy

2.3. Synthesis of zeolite powder

By keeping the silica alumina ratio of zeolite same as clay, the conversion of Montmorillonite clay (silica and alumina source) to zeolite was carried out by performing a series of experiments. The clay suspension was prepared by adding measured amount of clay and distilled water in a glass beaker. A stirring bar was immersed into the solution and stirred with a magnetic stirrer (SCHOTT Instruments GmbH) at 200 rpm for 30 min. Measured amount of NaOH aqueous solution was slowly mixed to clay suspension with constant and vigorous stirring, the mixture turned thin mud like sol. The mixture was stirred for 1 h. All these procedures were carried out at room temperature. The resulting mixture was sonicated for different time from 0.5 h (30 min) to 8 h. The ultrasound equipment (UIP1500 hd HIELSCHER Ultrasound Technology) which produces acoustic waves at frequency of 20 kHz [25]. The energy input of sonication was 250 W followed by aging for 1 day to 15 days. The molar composition of the sol used for the synthesis was 50 Na_2O: 1 Al_2O_3: 2.5 SiO_2: 1000 H_2O. In order to increase the reaction rate, decalin and hydrogen peroxide solution was added separately into the reaction mixture and their effect in zeolite formation by sonochemical process was studied.

In Sonication mediated hydrothermal process, the sonicated mixture was poured into Teflon-lined stainless steel autoclave. Hydrothermal crystallization was continued under autogenous pressure in a hot air oven at 100 °C for 12 h, 24 h and 48 h. After synthesis, the zeolite powders were washed thoroughly with deionized water until the pH of the washing liquid became neutral and then dried at room temperature for further characterization.

For comparison, different clay suspensions with NaOH solution were treated by hydrothermal process similar to above mentioned condition without sonication treatment. The molar composition of the initial sol was same as that used in case of sonochemical synthesis. Crystallization was carried out in oven at 100 °C. The powdered products were recovered through centrifugation, washed with DI water until pH < 8. The details of batch composition and condition are described in Table 1.

2.4. Preparation of zeolite membrane on clay-Al_2O_3 support

An indigenous clay–Al_2O_3 tube of diameter 10 mm, thickness 3 mm and 100 mm length was used as support for synthesis of the zeolite membrane derived from clay suspension. Before membrane preparation, the substrates were cleaned with acetone in an ultrasonic cleaner (Vibracell, USA) for 10–15 min to remove the dust particles and oily matter. The outer surface of the support tubes were wrapped with Teflon tape so that the zeolite layer was formed inside the tube. The support was modified by cationic polymer PolyDADMAC (0.5 wt% in 20 mL of H_2O) and dried at 60 °C for 30 min leading to DADMAC polycations adsorbed on the clay − alumina support surface. The seed monolayer was deposited on the polymer modified support surface. The support was dipped in a 3% zeolite seed suspension synthesized from Mt clay as raw material. The seeded supports were placed vertically in an ultrasonically irradiated solution having composition similar to zeolite formulation with 8 h sonication with 8 M NaOH solution and kept for 72 h (3days) to 360 h (15 days) aging in reaction mixture. After synthesis, the zeolite coated membrane was washed thoroughly with deionized water until the pH of the washing liquid became neutral. The synthesized membrane was dried in hot air oven at 60 °C for overnight.

For comparison the membrane was synthesized by conventional method. In that case the seeded support tube was exposed to

Table 1
Batch Formulation for Zeolite from clay suspension.

Experiment No	Strength of NaOH	Sonication Time	Hydro-thermal Time (at 100 °C)	Aging Time
1	0.5 M	–	24 h	
2	0.5 M	–	48 h	
3	0.5 M	30 min	12 h	
4	1.0 M	30 min		
5	1.0 M	1 h		
6	1.0 M	2 h		
7	1.0 M	4 h		
8	8.0 M	6 h		3 d
9	8.0 M	6 h		7 d
10	8.0 M	6 h		15 d
11	8.0 M NaOH	8 h		15 d
In addition two more composition was studied				
12	Decalin	4 h		
13	H_2O_2	4 h		

Table 2
Chemical composition of clay used in this study.

Oxides	SiO_2	Al_2O_3	Fe_2O_3	TiO_2	CaO	MgO	Na_2O	K_2O	L.O.I.
% (w/w)	50.46	20.64	12.59	1.69	0.69	1.81	1.79	0.67	9.58

hydrothermal treatment in an autoclave. The autoclave was filled with reaction mixture having same composition containing clay suspension. The hydrothermal treatment was continued at 100 °C for 12 h.

2.5. Characterization

Table 2 summarizes the chemical compositions of original Bentonite clay. The contents of the components were determined by chemical analysis and the chemical composition was presented in the form of corresponding oxide. The particle size distribution of the clay was determined with a laser scattering particle size distribution analyzer (Malvern Zetasizer, Nano series, UK). The Crystalline structure of the as synthesized powder was determined by X-ray diffraction pattern in the 2θ range of 0–60° were collected at ambient temperature. XRD was carried out on a Philips 1710 diffractometer using CuK_α radiation (α = 1.541 Å). The FTIR spectra of the clay and zeolite crystals were recorded in the diffuse reflectance mode using a Nicholet 380 FTIR spectrophotometer for detecting characteristics vibration bond. Thermogravimetric analyses (TGA) and differential thermal analyses (DTA) were performed in static air using the thermogravimetric analyzer (NETZSCH STA 409C F3 Jupiter, Germany). The samples were heated at a rate of 10 $^0C\ min^{-1}$ under air flow. Microstructure and morphology of the zeolite crystals and membranes were examined using Scanning electron microscopy (FESEM: model Leo, S430i, U. K.). Elemental analyses of the samples were conducted by energy dispersive X-ray spectrometer (EDXS) attached to a Cambridge Stereo scan S440 microscope. The porous properties of the zeolite were evaluated by N_2 adsorption/desorption measurements at 77 K on a volumetric gas adsorption analyzer (Autosorb-iQ-MP, Quantachrome). The samples (~50 mg) were appropriately outgassed (~24 h at 250 °C) under high vacuum followed by adsorption of ultra-pure N_2 (99.9999%) while He (99.999%) was used as carrier gas. The specific surface area values were calculated by the Brunauer- Emmett- Teller (BET) method. The micropore volumes were determined using the BJH (Barret-Joyner-Halenda) method. Pore size distributions were deduced by using the N_2-adsorption at 77 K.

2.6. Gas permeation study

Gas permeation studies were done by a specially designed permeation cell developed in our laboratory (Fig. 1). For permeation experiments, the membrane was mounted in a stainless steel permeation cell and sealed between two silicon O-rings. Simultaneously, the leak test was carried out before the permeation experiment of each individual gas in order to obtain the correct data.

Single gas permeance of different gases like H_2, CO_2 and N_2 having different kinetic diameters were investigated. Soap film flow meter was used to measure the gas permeance of the membrane under the feed pressure of 100–300 KPa at 30 °C, using the formula,

$$\text{Permeance} = \text{Flux}/D_P$$

where D_P is the pressure difference between feed side and permeate side.

The selectivity of two gases G1/G2 was defined as the permeance ratio of gas G1 and G2. The gas permeation measurement of each single gas was repeated until the permeance data for the successive 10 tests were close. The single gas permeance was the average of 10 successive tests. The performance of the synthesized membranes was evaluated by measuring separation factor for CO_2 – CH_4 and H_2-CO_2 mixed gas. For mixture gas (CO_2-CH_4 and H_2-CO_2), separation factor was calculated from the area under the curve for each component in feed and permeate composition measured by gas chromatography (model – Trace GC ultra, serial no. 20092814, Thermo SCIENTIFIC, Germany). The separation factor $\alpha_{A/B}$ of the binary mixture permeation was calculated from equation (1)

$$\alpha_{A/B} = Y_A/Y_B/X_A/X_B \quad (1)$$

where x and y are the mole fractions of each component in the feed and permeate sides, respectively. Subscripts A and B refer to components A and B, respectively. The permeance measurements were carried out at the same experimental conditions such as same temperature and pressure difference.

3. Results and discussion

3.1. Bentonite clay

The main elemental composition of the clay materials was analysed and the results are presented in Table 2 which show SiO_2/Al_2O_3 ratios of 2.5 along with almost 12% of Fe_2O_3. The SiO_2/Al_2O_3 ratio of the feedstock is of paramount importance.

Fig. 2a and b shows the XRD pattern and FESEM micrograph of clay used in this study respectively. Due to nano-dimension and low crystallinity of these bentonite clays, XRD pattern reveals few low intense and broad reflections for the main clay mineral (Montmorillonite) along with some mixed layer clays (Illite-Smectite) and Kaolinite in the diffractogram (Fig. 2a). Even minor amount of quartz produce sharp intense XRD lines due to its high crystallinity. DTA/TG curve of the clay materials are shown in inset of Fig. 2a. The thermo gravimetric analysis of clay was done from room temperature to1000 °C. The clay sample exhibits a decomposition loss of 16.21% of weight at 1000 °C. The weight losses between 80 and 110 °C and 450–515 °C normally associated with removal of surface water and dehydroxylation of the clay material respectively. The differential thermal analysis curve shows two small endothermic peaks around 100 °C and 800 °C and a small exothermic peak 500 °C. The peaks at around 100, 500 and 800 °C corresponding to the loss of water of hydration, dehydroxylation of the clay material and the carbonate decomposition respectively (inset of Fig. 2a) [26]. The FESEM image (Fig. 2b) reveals only the presence of Montmorillonite clay with typical nano-plate like grains, while angular grains of quartz are rare. [27]. Accordingly the processed bentonite clay is established as a Montmorillonite clay (Mt) -which is used for synthesis of zeolites throughout this research work. Particle size distribution curve of the clay showed a mono modal particle size distribution having d_{50} value approximately 350 nm (inset of Fig. 2b).

3.2. Zeolite powder

Fig. 3a–c depicts the XRD patterns of the different powders formed after ultrasonic irradiation followed by hydrothermal treatment of clay in presence of NaOH. Hydrothermal reaction was carried out at 100 °C for 24 h and 48 h (Fig. 3a and b respectively). Fig. 3c shows the XRD pattern of same reaction mixture after 30 min of ultrasonic irradiation followed by hydrothermal treatment for 12 h at 100 °C. It is clear from the XRD pattern that JBW zeolite was formed after 30 min of sonication and hydrothermal treatment for 12 h at 100 °C [28]. After addition of 0.5 M NaOH solution with 24 h hydrothermal at 100 °C, two peak of JBW (0 1 0) and (0 1 1) were obtained. With increasing the time period of hydrothermal treatment to 48 h, more peaks were appeared but 30 min sonication treatment followed by hydrothermal for only 12 h resulted pure phase of JBW with higher crystallinity.

To investigate the morphology of the synthesized zeolite powders FESEM micrographs were analyzed. Inset of Fig. 3a–c show the FESEM micrograph of zeolite synthesized from clay in different synthesis condition respectively. Inset of Fig. 3a describes the morphology of the

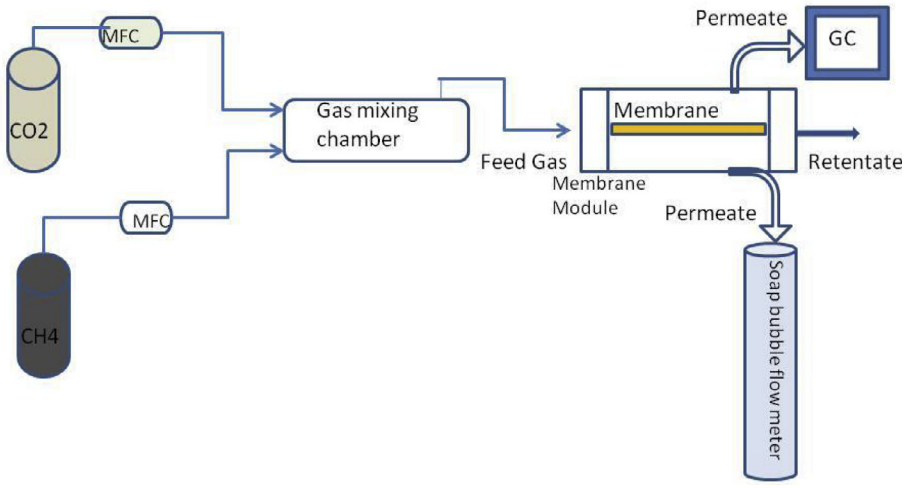

Fig. 1. Schematic presentation of gas permeation set up.

JBW zeolite obtained by transformation of Mt clay to zeolite. From the FESEM micrograph it can be seen that after 24 h hydrothermal treatment at 100 °C of clay suspension with 0.5 M NaOH diamond shaped crystals of JBW phase were started to form. After 48 hr hydrothermal treatment at the same temperature the crystallinity of JBW products improves, while the crystal morphology of the zeolite obtained also shows the same nature (inset Fig. 3b). Same type of crystal morphology was also obtained by 30 min sonication followed by only 12 h hydrothermal treatment (inset Fig. 3c). The gradual decrease in time of hydrothermal process with the application of ultrasonic irradiation indicates that the phase pure zeolite structure formation may be possible without hydrothermal treatment by adjusting the time of ultrasonic irradiation followed by aging treatment using alkaline medium at room temperature.

Based on the observation of formation of zeolite by ultrasonic irradiation, clay suspension was sonicated for different time starting from 0.5 h, 1 h, 2 h and 4 h under the sonication energy of 250 W, and aging time for 24 h at room temperature. The same was compared with zeolite formed after 4 h sonication in presence of decalin and H_2O_2 in reaction medium in separate experiments. On sonication treatment of Mt clay with different amount of NaOH, different zeolite composition was obtained. Initially only 0.5 M NaOH solution was added 10 g of clay suspension to get a molar composition of zeolite JBW where Na_2O/SiO_2 is 0.72 [29]. Si-Al containing solutions at lower alkalinity produced JBW-type zeolite (also known as Na-J) [30].

Fig. 4a–f illustrates the XRD patterns of the synthesized zeolite samples with different sonication time, ranging from 0.5 h to 4 h. With 30 min and 1 h sonication of clay with NaOH did not exhibit any characteristic peaks of zeolite. When the sonication time increased to 2 h two characteristic peaks of NaP (JCPDS no. 71–0962) zeolite (1 0 1), (3 0 1) was detected. After 4 h sonication NaP zeolite was detected as the dominant phase (JCPDS No. 71-0962). Moreover, the formation of NaP phase at Na_2O/SiO_2 molar ratio 1.1 could be discussed in terms of the role of OH^- groups in increasing the nucleation rate of NaP zeolite, which properly accounts for the dissolution of the amorphous gel and the formation and release of NaP zeolite hetero-nuclei at the gel-solution interface. This may lead to an effective acceleration of the crystal growth and shorten the induction period for the crystal growth of NaP zeolite [31–34]. Thus, a requisite concentration of sodium hydroxide and the duration of sonication time are needed to tune the composition of the starting gel for crystallization of NaP zeolite. To investigate the role of sonication effect and presence of NaOH in the formation of NaP phase, experiments were done by adding 10 mL of trans decaline and H_2O_2 in two separate experiments in clay suspension without adding NaOH during sonication. It is interesting to note that when trans decaline and H_2O_2 was used in absence of NaOH, NaP phase was

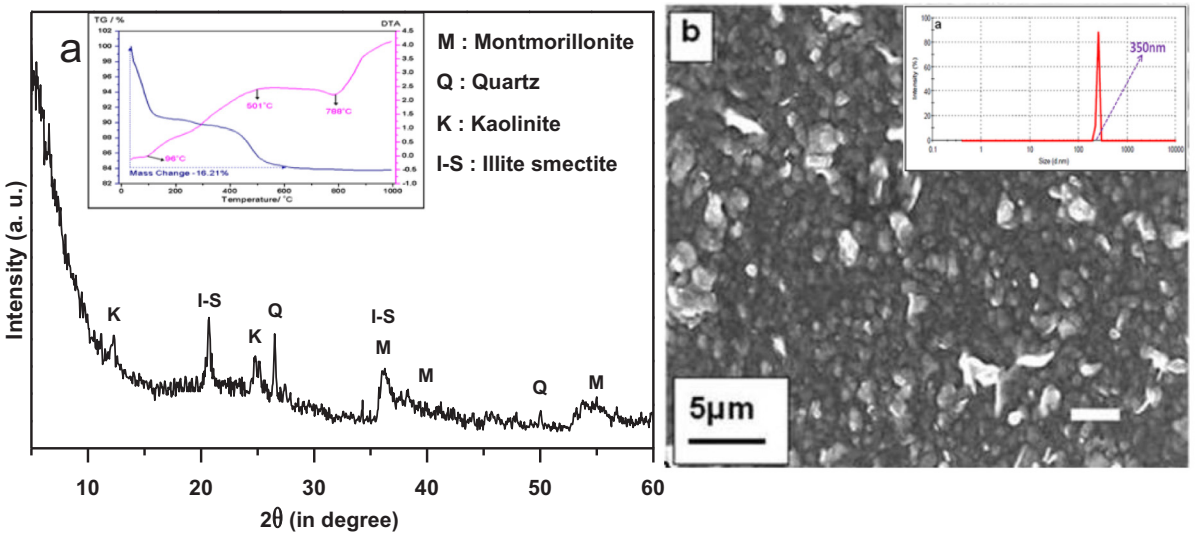

Fig. 2. (a) XRD pattern of clay (inset: DTA-TGA analysis) (b) FESEM micrograph of untreated Clay (inset: particle size distribution of the same).

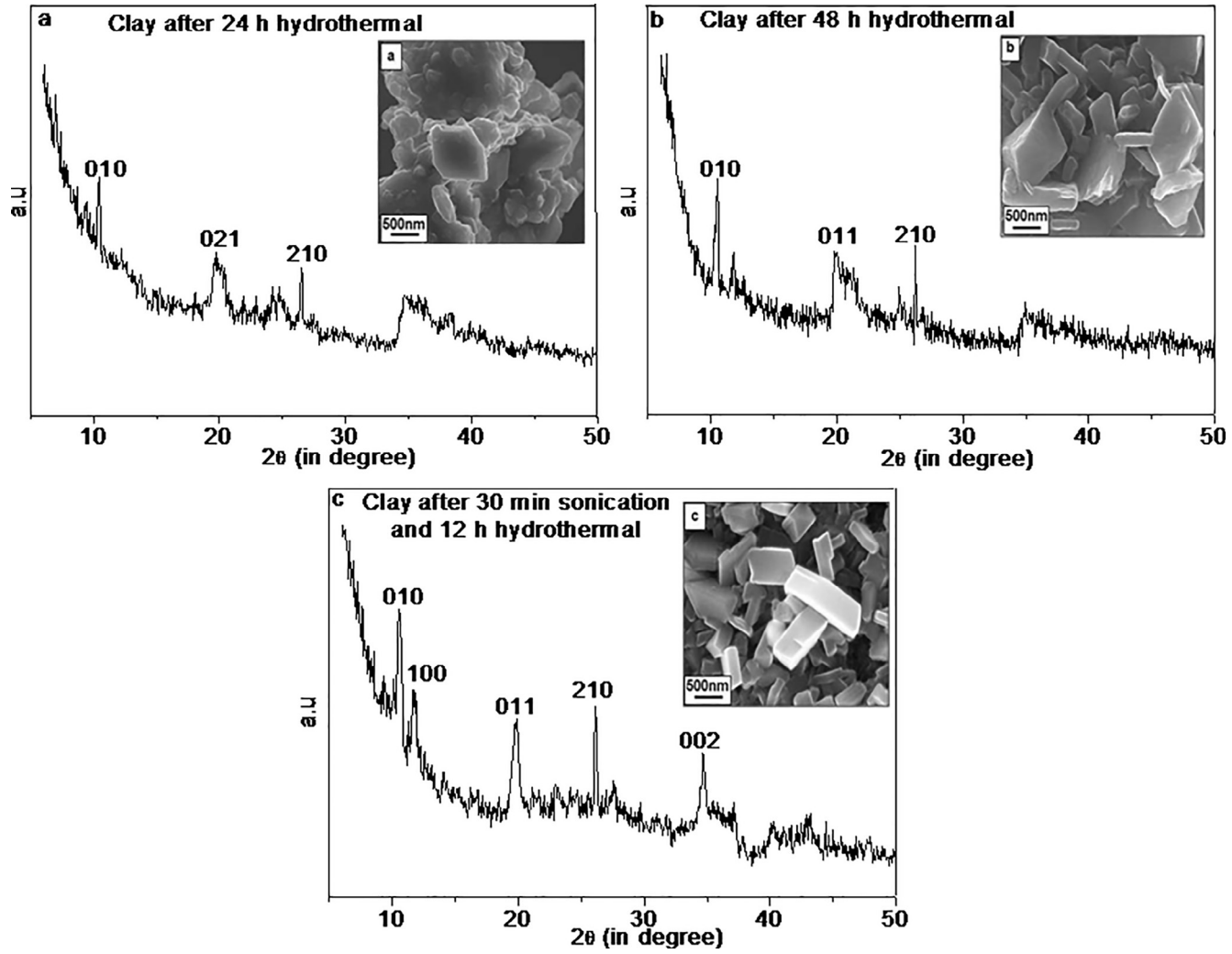

Fig. 3. XRD pattern of powders obtained from clay by (a) 24 h hydrothermal, (b) 48 h hydrothermal and (c) 30 min sonication followed by 12 h hydrothermal, with 0.5 M NaOH at 100 °C. Inset of each figure shows the representative FESEM micrograph of the zeolite powder.

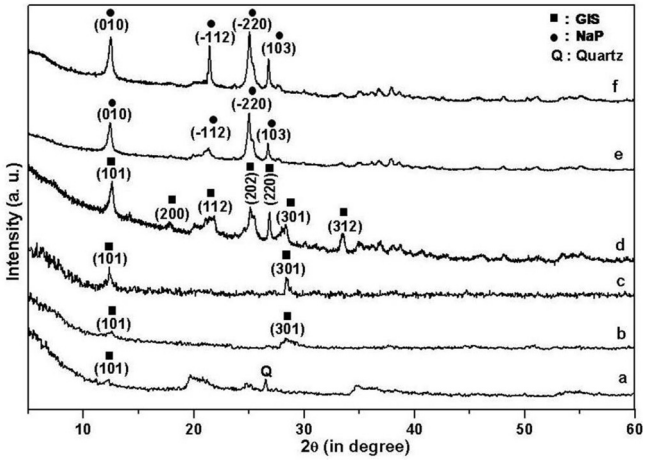

Fig. 4. XRD pattern of synthesized zeolite from clay by sonication irradiation for (a) 30-minute, (b) 1 h, (c) 2 h and (d) 4 h with 1 M NaOH, (e) 4 h with decaline, (f) 4 h in H_2O_2.

predominant (Fig. 4e and f). The significant increased in crystallinity of the produced NaP phase and formation can be explained on the basis of effect of ultrasound. The chemical effect of high-intensity ultrasound results primarily from acoustic cavitation: the formation, growth, and implosive collapse of bubbles in liquids [35–37]. It has been reported in literature that the maximum temperatures reached during collapsing of bubble can reach up to 2600 °C on the local spot [38]. This sonication effect generates aluminum deficient forms and by controlling the duration of sonication, different Si/Al ratios can be achieved [39].

The FESEM images of the zeolite obtained by 0.5 h (30 min) to 4 h sonication of Mt clay mixture are shown in Fig. 5a–f. As discussed earlier, it was confirmed that finally NaP phase was formed after 4 h Sonication. Though the phase transformation of clay suspension to NaP zeolite was started after 0.5 h sonication with 1.0 M NaOH, but the crystal morphology of the synthesized product didn't show any difference (Fig. 5a–b). After 2 h sonication at same reaction condition, the change in morphology has been observed (Fig. 5c). NaP zeolites form plate-like aggregates about which turns into typical woolen ball structure with a length of 1–2 μm. Such habits are characteristic for gismondite group of zeolites. From Fig. 5d it was confirmed that, finally after 4 hr sonication the clay suspension completely transformed to NaP type zeolite. Further the same reaction was also done in done using decaline and hydrogen peroxide. In sonochemical reaction, ultra sound enhanced the chemical reaction in acoustic media by acoustic cavitation. Cavitation is the formation, growth and collapse of the bubbles. According to literature, radicals produced from the aqueous cavitation may be the main source of pressure and temperature. High temperature ~2000 °C and pressure ~1000 bar produced during collapsing of bubbles may supply energy to break the chemical bonds and return

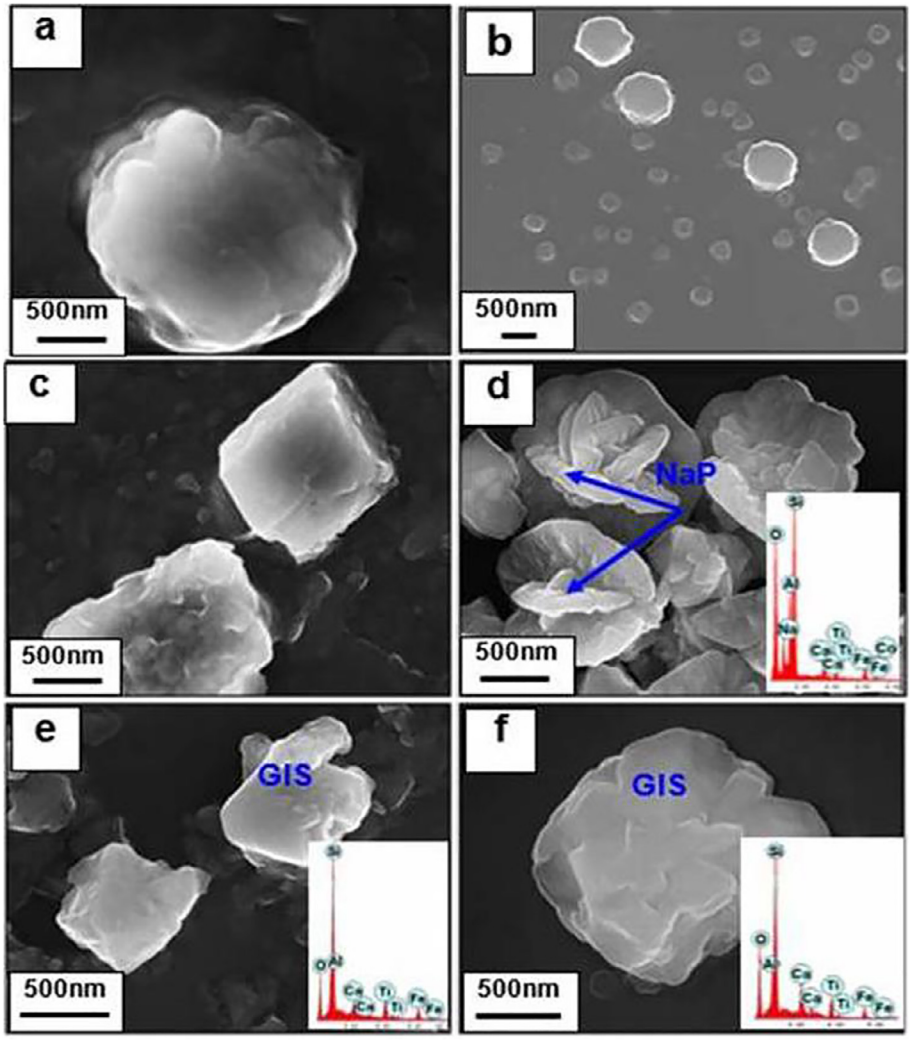

Fig. 5. FESEM micrograph of synthesized zeolite from clay by sonication irradiation for (a) 30-minute, (b) 1 h, (c) 2 h and (d) 4 h with 1(M) NaOH, (e) 4 h with decaline, (f) 4 h with H_2O_2 (inset shows corresponding EDX).

back the charge radicals into bulk solution [40].

In our work we have chosen decaline and H_2O_2 based on reported literature. Decaline produces high energy acoustic cavitation because its low vapour pressure [41] on the other hand the HO radical forms as the intermediate species during decomposition of H_2O_2 [42]. H_2O_2 in presence of ultrasound assumed to react in the following process

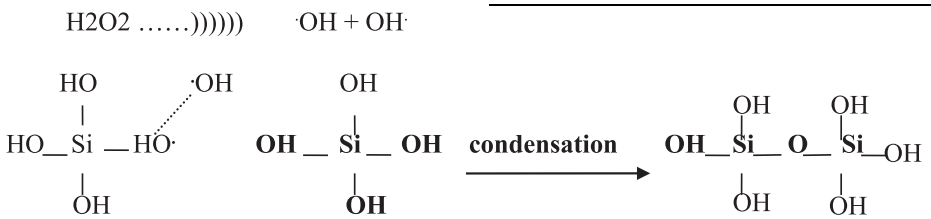

The above reactions describe the starting of zeolization from silica source. The reaction involving the condensation between silica molecule may be the initiation of the zeolite formation. The OH radical produced from H_2O_2 decomposition increases the rate of reaction. The morphology of the obtained products is shown in Fig. 5e and f respectively. From the EDX data it is clear that after 4 h sonication of Mt clay with trans decaline and H_2O_2 due to absence of available Na^+ ion GIS phase is formed containing Ca^{+2} (from clay) instead of NaP phase.

Fig. 6 reveals the XRD patterns of the synthesized zeolites after adding the 8.0 M NaOH solution to the initial composition of clay and performing 6 h to 8 h sonication followed by aging. As shown in Fig. 6a–c the characteristic peaks of sodalite at (1 1 0), (2 1 1), (3 1 0), (2 2 2) and (3 3 0) can be identified (JCPDS No. 89-9099). After 6 h sonication, with increasing the aging time the crystallinity of the sodalite phase were also increased. The formation of sodalite phase by using higher molar concentration of NaOH in same reaction condition may be the presence of higher concentration of sodium ion and pH favored sodalite crystallization [43,44]. Finally when the clay suspension was sonicated for 8 h with 8.0 M NaOH solution followed by 15 days aging, phase pure more stable, LTA (Zeolite-4A) was formed with high crystallinity. Fig. 6d shows the XRD pattern of LTA zeolite. Peaks at (2 0 0), (2 2 0), (2 2 2), (6 2 2) etc confirms the formation of

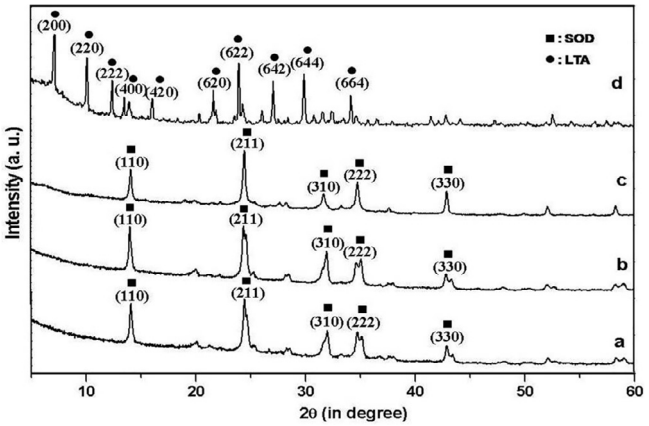

Fig. 6. XRD pattern of synthesized zeolite by sonication irradiation for 6 h with 8 M NaOH followed by aging for (a) 3 days, (b) 7 days, (c) 15 days, and (d) for 8 h with 8 M NaOH followed by 15 day aging.

well defined LTA phase (JCPDS No. 73-2340).

The FESEM images of the products formed in the last set of experiments were shown in Fig. 7a–d. In these batches the clay suspensions were sonicated for 6–8 h with 8.0 M of NaOH followed by different aging time at room temperature. The FESEM micrograph indicates the morphology of the synthesized zeolite as spherical particles (Fig. 7a–c) and Fig. 7d shows the characteristic cubic shape LTA zeolite [45–47]. A schematic representation of the probable steps of the zeolite synthesis processes starting from Montmorillonite clay to JBW, NaP, SOD and LTA (abbreviation of zeolite names were collected from IZA [28]) zeolite formation are shown in Fig. 8. Fig. 8a shows the schematic layer structure of the Mt clay material having an octahedral sheet containing different elements (Mg, Fe, Al) and OH-groups, sandwiched between two tetrahedral sheets with Si-O tetrahedrons. During ultrasonic irradiation of clay suspension with NaOH solution, individual plates of clay were separated from each other. Further sonication broke the clay structure and significant dissolution of alumina and silica species took place. The important step of zeolite formation i.e. sol to gel transformation was initiated during sonication of the mixture in presence of the Na^+ in the solution and the composition close to the corresponding zeolite stoichiometry started to form to start the nucleation of zeolite. This might be the starting point of formation zeolite from the amorphous precursor material. The changes in the system, induced by the presence of combined Na^+ and OH^-, hydration and dissolution of the alumina and silica species along with solution-mediated transport may be the cause of zeolite nucleus formation. The initial sonication period took up half of the entire crystallization duration, which was the consequence of the inhomogeneous distribution of the reactants in the initial gel [48].

In sonochemical reaction, evolution of huge energy during collapsing of bubbles helps in the formation of free radical, and activates the reaction species which helped in the nucleation and growth of colloidal nano particles of the reaction products [49]. During crystallization, the first stage proceeds through the reorganization of the amorphous alumina silicate unit formed during the sonication process of precursor. The reorganization involved a formation of Si-O-Al bond and reorientation of bond angle. The crystallization process takes place in the small volume of aggregate into the gel phase. After this stage, the growth in the system is dominated by solution mediated transport which formed well shaped zeolite crystal. The aggregation and rearrangement of the secondary particles lead to the formation of the final nano sized zeolite crystals. As per crystallization theory, zeolite growth has been found to be affected by a multitude of parameters such as sonication irradiation power, irradiation time, gel composition aging time etc [50]. The details of XRD and FESEM study show that the transformation of clay to zeolitic phase started forming at room temperature under 250 W sonication energy after 30 min sonication

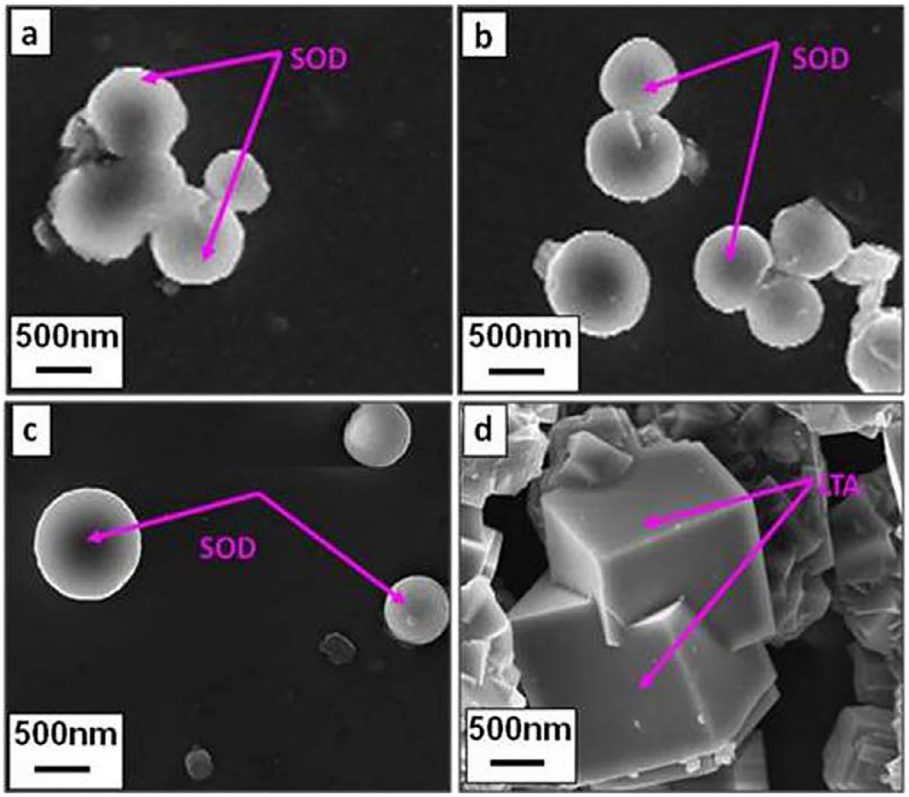

Fig. 7. FESEM micrograph of synthesized zeolite by sonication irradiation for 6 h with 8 M NaOH followed by aging for (a) 3 days, (b) 7 days, (c) 15 days, and (d) for 8 h with 8 M NaOH followed by 15 day aging.

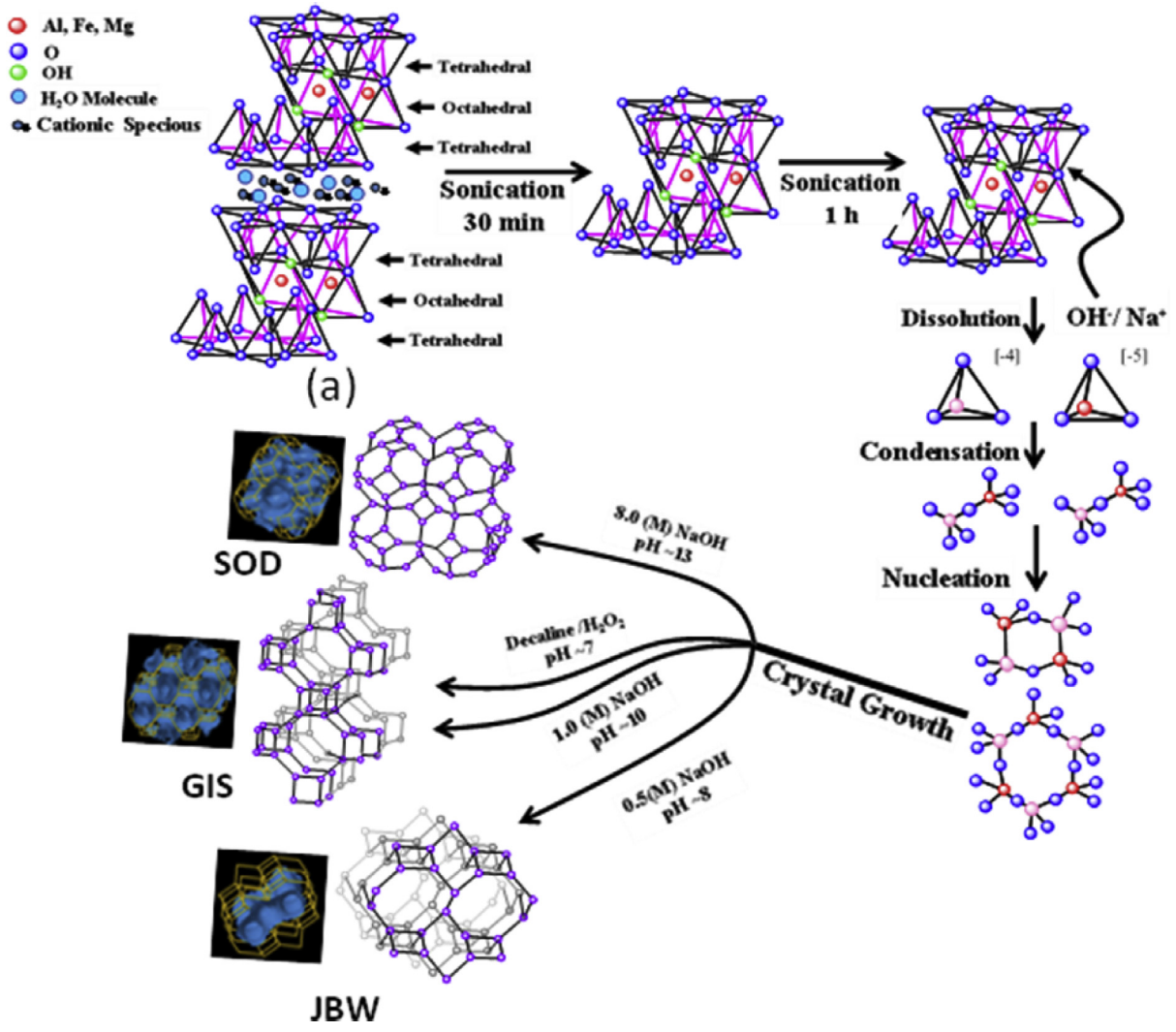

Fig. 8. Schematic representation of conversion of clay to zeolite.

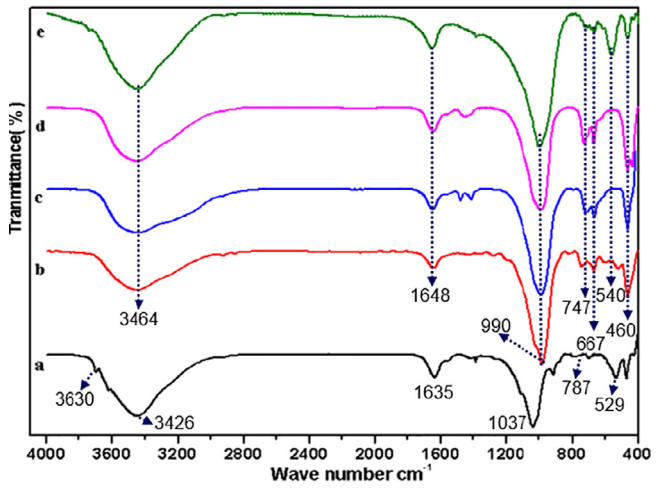

Fig. 9. FTIR spectra of clay (a) untreated (b) for 30 min sonication with 0.5 M NaOH followed by 12 h hydrothermal at 100 °C, (c) 4 h sonication with 1 M NaOH, (d) 6 h sonication with 8 M NaOH followed by 15 days aging and (e) for 8 h sonication with 8 M NaOH followed by 15 days aging.

irradiation.

The transformation of clay to aluminosilicate framework in the zeolites by sonication in presence of NaOH can be confirmed by FTIR analysis (Fig. 9a–e). Fig. 9a shows the typical FTIR spectra of Mt clay. In Fig. 9a bands were observed for the signals at 3430 and 3626 cm^{-1}, which are due to stretching bands of the OH groups, 1635 cm^{-1} which is assigned to the OH deformation, 1037 cm^{-1} assigned to the Si–O vibrations within the layer and the band at 529 cm^{-1} from the Si–O–Al, where Al is an octahedral cation [51]. In Fig. 9b–e the bands in the region of 460–500 cm^{-1} are related to internal tetrahedron vibrations of Si-O and Al-O of the synthetic zeolites. The characteristic zeolite bands appeared on the spectra, including the asymmetric Al-O stretch located in the region of 990–1000 cm^{-1}, and their symmetric Al-O stretch located in the region of 660–750 cm^{-1} [52]. The bands in the region of 500–550 cm^{-1} are related to the presence of the double rings (D4R and D6R) in the framework structures of the zeolitic materials. These features confirm the presence of zeolitic material [53,54]. The Asymmetric T-O stretching vibrations of zeolite JBW framework structure are observed around 970 cm^{-1} and symmetric stretching vibrations of Si–O and Al– O were noticed at, 747 and 667 cm^{-1} [55]. The symmetric stretching vibrations of zeolite NaP framework structure of Si–O and Al– O were noticed at, 667 and 729 cm^{-1} [56]. The bands

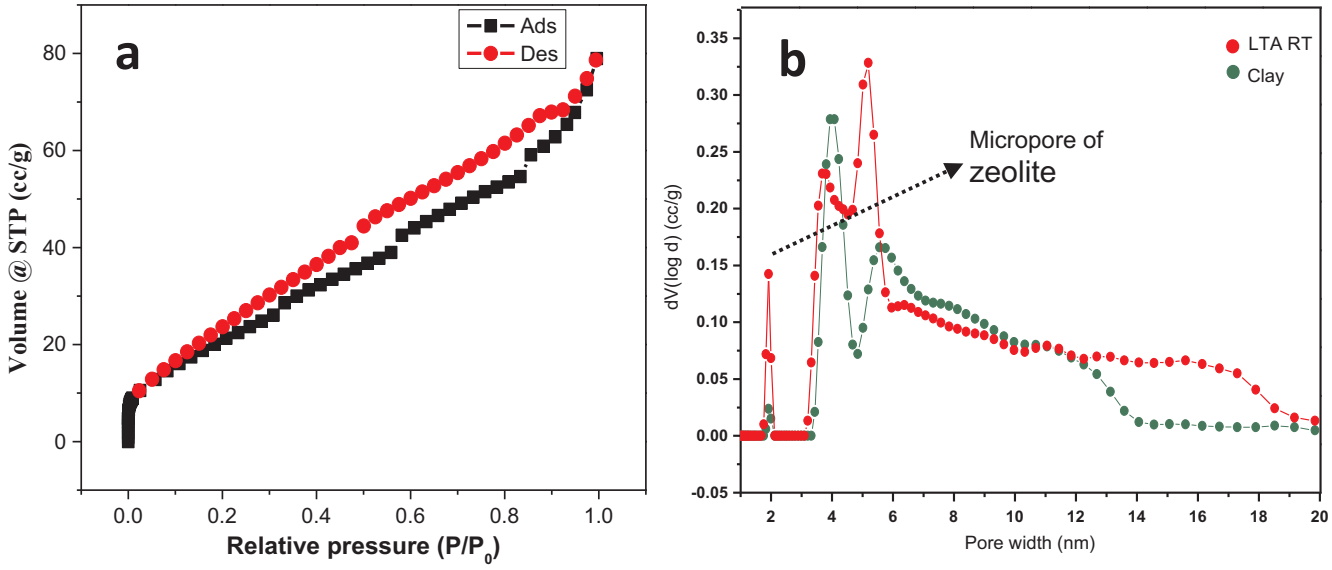

Fig. 10. (a) Nitrogen adsorption – desorption isotherm (b) BJH pore size distribution of LTA zeolite at room temperature and raw material clay.

with a maximum at 1648 cm^{-1} are peculiar of vibrations of functional groups of OH type and are ascribed to water with zeolitic nature. Similar behavior was found by Albert et al [57]. The transmittance of the asymmetric stretch of the Si-O-Al in the SOD framework consists of a single band at 980 cm^{-1} and the 541 cm^{-1} band is due to D4R which is the major secondary building unit in LTA zeolite [58,59]. From the FTIR results it was also confirmed that by sonication treatment of clay suspension different zeolite phases were formed. Montmorillonite clay may be a promising source of silicon and aluminum for the synthesis of aluminosilicate zeolite. Fig. 10a and b describes the characteristics nitrogen adsorption –desorption isotherm of LTA zeolite synthesized from clay materials at room temperature (Fig. 10a) and their pore size distribution (Fig. 10b). The BET surface area of clay powder and LTA zeolite obtained are 74 m^2/g and 287 m^2/g respectively. The pore size distribution calculated by using the BJH methods is shown in Fig. 10b. The pore size distribution curves show the narrow size distribution of LTA zeolite (synthesized at room temperature). From the above discussion, it was observed that zeolite powder was successfully synthesized from montmorillonite clay by ultrasonic irradiation at room temperature. Based on that observation, membrane was synthesized at room temperature on low cost clay alumina support tube by sonochemical method.

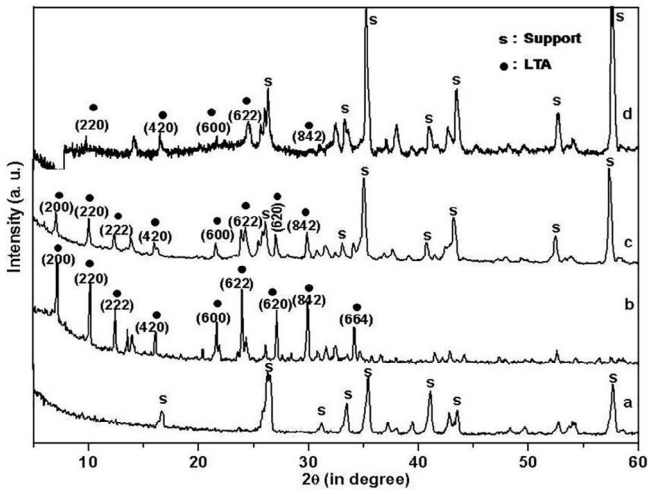

Fig. 11. XRD pattern of (a) Clay-A_2O_3 support, (b) LTA zeolite powder, (c) LTA membrane on Clay-Al_2O_3 support for12 h hydrothermal at 100 °C and (d) LTA membrane on Clay-Al_2O_3 support at room temperature.

3.3. LTA zeolite membrane

The formation of phase pure LTA membranes was confirmed by XRD analysis. Fig. 11a–d show the XRD patterns of the clay-Al_2O_3 substrate, LTA zeolite powder, LTA membrane layer synthesized on the substrate by hydrothermal method along with at room temperature respectively. From the XRD pattern, the LTA membrane layer prepared on the support (Fig. 11c) shows that all diffraction peaks of the LTA zeolite, and the hkl-values, i.e. (2 0 0), (2 2 0), (2 2 2), (4 2 0), (6 0 0), (6 2 2), (6 2 0), (8 4 2), and (6 6 4) are in agreement with those LTA zeolite crystal besides the clay-Al_2O_3 signals from the support.

Fig. 12a–d shows the FESEM micrograph of membrane surface morphology and corresponding cross sectional view along with line scanning and elemental mapping of constituent elements of LTA membrane synthesized at room temperature by sonochemical method and by hydrothermal method at 100 °C for 12 h. Fig. 12a and b confirms the formation of LTA zeolite membrane on clay-Al_2O_3 support tube at room temperature by sonication treatment of clay. FESEM micrograph of surface morphology of the membrane layer shows that the interlock structure of LTA membrane was spontaneously form on the seeded support at room temperature from the 8 h sonicated clay suspension on 15 days aging. The corresponding cross sectional view shows a uniform membrane layer with 10 μm thickness. To confirm the formation of the LTA membrane on support at room temperature by only ultrasonic irradiation effect from Mt clay and NaOH solution, FESEM, EDS elemental mapping (O, Na, Al, Si, Ca and Fe) of the membrane surface layer and corresponding line scanning of the cross sectional view were done and the results are shown in Fig. 12b. It can be seen from the elemental mapping of the surface layer (Fig. 12b), uniform membrane layer was formed at room temperature. Weak signals of Ca and Fe in the mapping came as impurity from clay material. During line scanning, sodium peak intensity is higher when the scanning was started at the membrane layer and no sodium peaks were detected for the support layer, which proved that the membrane layer was formed on support surface only. In Fig. 12c the FESEM microphotograph of the LTA membrane synthesized by hydrothermal method reveals that many small cube-like interconnected zeolitic crystals formed by hydrothermal treatment. Fig. 12d shows the membrane cross-section and it confirms that LTA membrane is formed as a homogeneous crystalline layer with

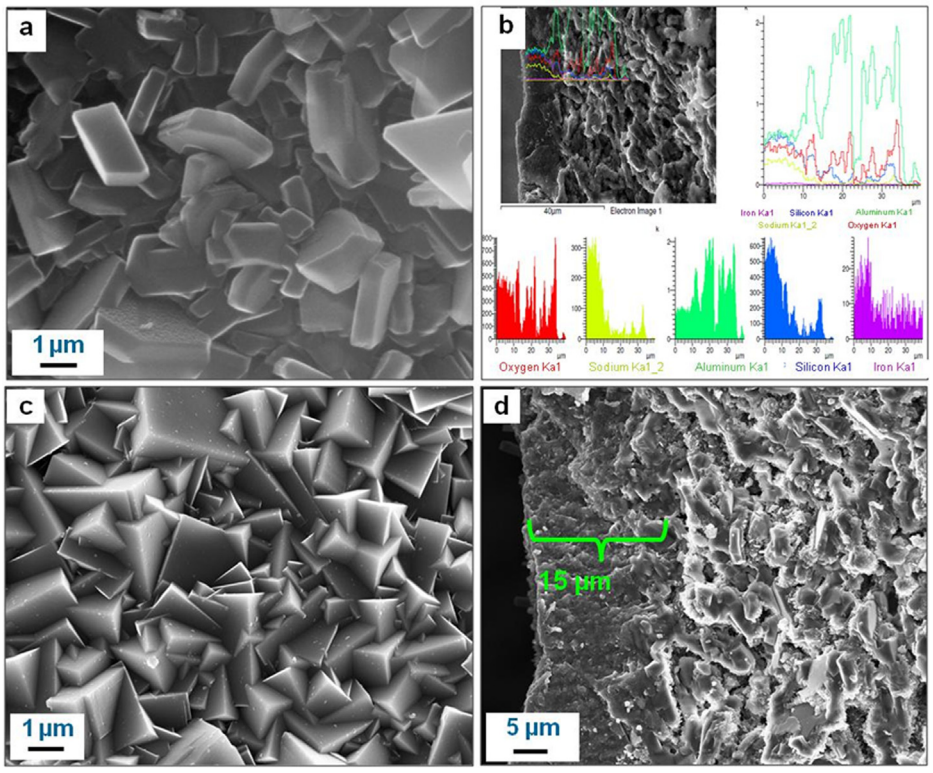

Fig.12. FESEM micrographs of LTA membrane (a) surface morphology (b) cross section and EDS elemental mapping (O, Na, Al, Si, Ca and Fe) and corresponding line scanning of the membrane layer synthesized at room temperature C) surface morphology and (d) cross sectional view of LTA membrane synthesized by conventional by hydrothermal method.

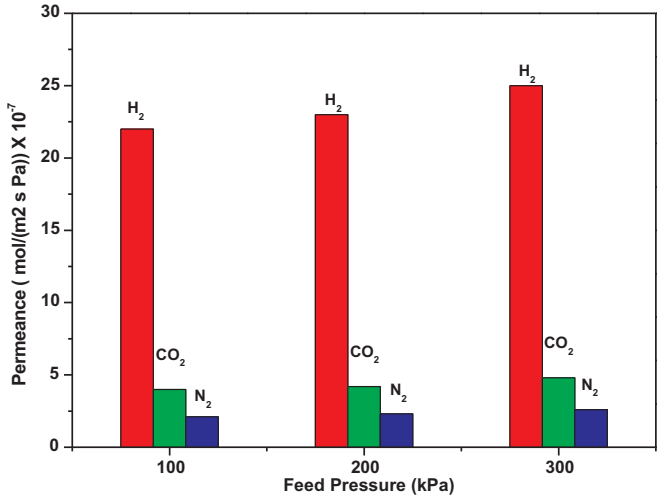

Fig. 13. Permeation results of LTA membrane for H_2, CO_2 and N_2 single gas as a function of different feed pressures. (Flow rate 200 mL min^{-1} at 30 °C).

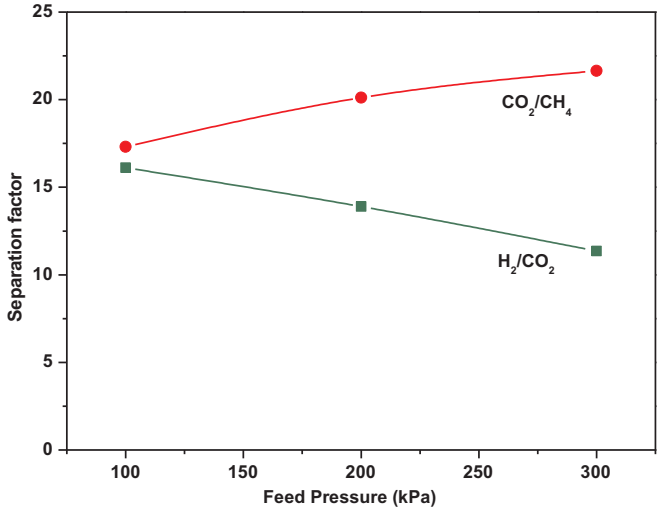

Fig. 14. Separation factor of LTA membrane for H_2-CO_2 (50:50) and CO_2-CH_4 (45:55) mixed gas as a function of different feed pressures.

15 µm thickness [60]. To end with this vital explanation, it can be concluded that preparation of LTA membrane layer on the support surface by sonochemical method at room temperature is possible for gas separation applications.

The quality of the synthesized membrane was finally evaluated from the gas permeation properties of the membrane. The membrane was mounted in a gas separation setup developed by us in our laboratory and used for gas separation studies. Single gas permeation of H_2, CO_2 and N_2 was measured at room temperature at different feed pressures and described in Fig. 13. The permeation of gas through the micropores of the zeolite can be explained by an adsorption–diffusion, molecular sieving mechanism where the permeance of the membrane is expressed as the rate of diffusion of the permeating species through the unit area of the zeolite membrane under the concentration gradient between feed and permeate side of the membrane." The synthesized LTA membrane shows a relatively high H_2 gas permeation value as compared to CO_2 and N_2. The molecular kinetic diameters of H_2, CO_2 and N_2 are 0.29, 0.33 and 0.36 nm respectively, which are close to the pore size of LTA zeolite (0.38 nm). Due to the difference in molecular kinetic diameter, the rates of diffusion through the membrane pores are different for H_2, CO_2 and N_2. The diffusion rate of H_2 is faster than that of CO_2 and N_2. The single gas permeation mainly depends on the kinetic diameter of the gases. The rate of change of permeance with pressure is less for CO_2 and N_2 than H_2. At high pressure, CO_2 adsorbs more strongly on the LTA zeolite membrane surface than H_2 and the rate of desorption of CO_2 from the membrane surface also decreased as compared to H_2. As a result, the H_2–CO_2 selectivity gradually increases with respect to different feed pressures. More interestingly, at room temperature, the appreciable highest selectivity value for H_2–CO_2 was found to be 15.34

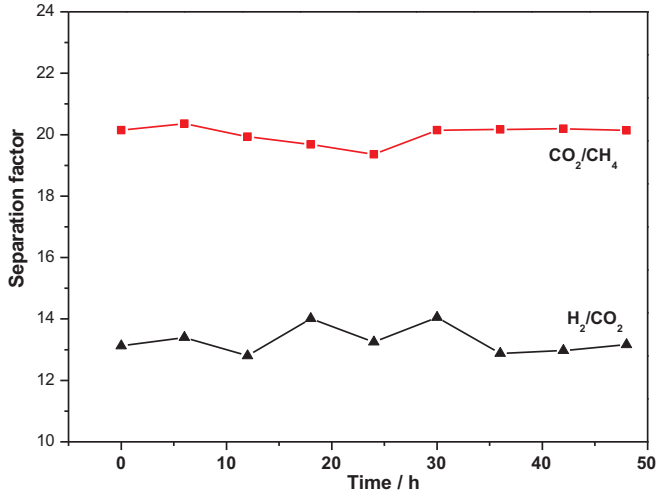

Fig. 15. Change of separation factor for H_2-CO_2 (50:50) and CO_2-CH_4 (45:55) as a function of time (h) for LTA membranes. (Flow rate = 200 mL min^{-1}, feed pressure = 200 kPa, permeation temperature = 30 °C).

at 300 kPa which was higher than literature values [61,62].

The real performance of the membranes can be investigated by their gas mixture separation ability. In the case of the H_2–CO_2 system, an appreciable separation factor value was obtained of 16.12 at 100 kPa and separation factor gradually decreased with increasing feed pressure, as shown in Fig. 14. This phenomenon can be explained by an adsorption–diffusion model. At higher pressure, CO_2 adsorbs more than H_2 because it has the strongest electrostatic quadruple moment and more adsorption sites are generated which block some of the adsorption of weak absorbing species. As CO_2 adsorbs preferentially in the LTA pore wall, it also desorbs and diffuses earlier than H_2 and the reasonable overall selectivity value was decreased. In CO_2-CH_4 gas mixture separation, a selectivity value of 20.91 was achieved and increased to a small extent with respect to the feed pressures.

Fig. 15 describes the change of separation factor for H_2-CO_2 and CO_2-CH_4 as a function of time (h) for LTA membranes. To evaluate the reproducibility, separation selectivity of H_2–CO_2 and CO_2-CH_4 as a function of different time intervals at constant pressure were carried out. The selectivity values were performed at high values and remain almost constant up to 48 h. The high reproducibility was due to the formation of defect-free pure LTA membrane layers.

4. Conclusion

In conclusion, here we present a concept and established for first time the fabrication of LTA membrane on clay alumina support at room temperature for H_2–CO_2, and CO_2-CH_4 separation. Using clay as starting material and formation of zeolite at room temperature by ultrasonic irradiation makes the process suitable for 'green synthesis. The adjustment of clay composition compare to zeolite Si/Al ratio, makes the method applicable to other types of zeolite for green synthesis. The work shows a good approach of the synthesis of membrane layer which could offer to be a safe, simple, and environmentally benign potential application for gas purification and production.

Conflict of interest

None.

Acknowledgements

The authors would like to thank DST WOS-A, India for financial supporting of the project SR/WOS-A/CS-1039/2014 and also thankful to Dr. K. Muraleedharan, Director, CSIR-CGCRI for his kind permission to publish the research work.

References

[1] P.E. de Jongh, Hydrogen storage: keeping out the oxygen, Nat. Mater. 10 (2011) 265–266.
[2] N.W. Ockwig, T.M. Nenoff, Membranes for hydrogen separation, Chem. Rev. 107 (2007) 4078–4110.
[3] A.K. Kohl, R. Nielson, Gas Purification, fifth ed., Gulf Publishing, Houston, TX, 1997.
[4] S. Sircar, T.C. Golden, Purification of hydrogen by pressure swing adsorption, Sep. Sci. Technol. 35 (2000) 667–687.
[5] J. Stocker, M. Whysall, G.Q. Miller, 30 Years of PSA Technology for Hydrogen Purification 2005, UOP LLC, Des Plaines, IL, 1998.
[6] R. Bredesen, K. Jordal, O. Bollard, High-temperature membranes in power generation with CO_2 capture, Chem. Eng. Process. 43 (2004) 1129–1158.
[7] S. Adhikari, S. Fernando, Hydrogen membrane separation techniques, Ind. Eng. Chem. Res. 45 (2006) 875–881.
[8] R.W. Spillman, Economics of gas separation membranes, Chem. Eng. Prog. 85 (1989) 41–62.
[9] M.E. Welk, T.M. Nenoff, F. Bonhomme, Defect-free zeolite thin film membranes for H_2 purification and CO_2 separation, in: E. van Steen, L.H. Callanan, M. Claeys (Eds.), Studies in Surfaces and Catalysis, Elsevier BV, NewYork, 2004, pp. 690–694.
[10] J. Lin, I. Kumakiri, B.N. Nair, H. Alsyouri, Microporous inorganic membranes, Sep. Purif. Meth. 31 (2002) 229–379.
[11] G.A. Ozin, A. Kuperman, A. Stein, Advanced zeolite materials science, Adv. Mater. 1 (1989) 69–86.
[12] E Drioli Tavolaro, Zeolite membranes, Adv. Mater. 11 (1999) 975–996.
[13] D.W. Breck, Zeolitic Molecular Sieves: Structure, Chemistry and Use, Wiley, New York, 1973.
[14] L. Ayele, J. Pérez-Pariente, Y. Chebude, I. Díaz, Conventional versus alkali fusion synthesis of zeolite A from low grade kaolin, Appl. Clay Sci. 132–133 (2016) 485–490.
[15] H. Faghihian, M. Kamali, Synthesis of Na-P zeolite from perlite and study of its ability to remove cyanide from liquid wastes, Int. J. Environ. Pollut. 19 (2003) 557–566.
[16] C. Belviso, F. Cavalcante, A. Lettino, S. Fiore, Effects of ultrasonic treatment on zeolite synthesized from coal fly ash, Ultrason. Sonochem. 18 (2011) 661–668.
[17] A.K. Dalai, N.C. Pradha, M.S. Rao, K.V.G.K. Gokhale, Synthesis and characterization of NaX and Cu exchanged NaX zeolites from silica obtained from rice husk ash, Indian J. Eng. Mater. Sci. 12 (2005) 227–234.
[18] A.Y. Atta, B.Y. Jibril, B.O. Aderemi, S.S. Adefila, Preparation of analcime from local kaolin and rice husk ash, Appl. Clay Sci. 61 (2012) 8–13.
[19] A.R. Loiola, J.C.R.A. Andrade, J.M. Sasaki, L.R.D. Silva, Structural analysis of zeolite NaA synthesized by a cost-effective hydrothermal method using kaolin and its use as water softener, J. Colloid Interface Sci. 367 (2012) 34–39.
[20] S. Chandrasekhar, P.N. Pramada, Investigation on the synthesis of zeolite NaX from Kerala kaolin, J. Porous Mater. 6 (1999) 283–297.
[21] L.V.C. Rees, S. Chandrasekhar, Hydrothermal reaction of kaolinite in presence of fluoride ions at pH < 10, Zeolites 13 (1993) 534–541.
[22] K.S. Suslick, S.B. Choe, A.A. Cichowlas, M.W. Grinstaff, Sonochemical synthesis of amorphous iron, Nature 353 (1991) 414–416.
[23] M.A. Beckett, I. Hua, Impact of ultrasonic frequency on aqueous sonoluminescence and sonochemistry, J. Phys. Chem A 105 (2001) 3796–3802.
[24] S. Askari, R. Halladj, ultrasonic pretreatment for hydrothermal synthesis of SAPO-34 nanocrystals, Ultrason. Sonochem. 19 (2012) 554–559.
[25] P. Pal, J.K. Das, N. Das, S. Bandyopadhyay, Synthesis of NaP zeolite at room temperature and short crystallization time by sonochemical method, Ultrason. Sonochem. 20 (2013) 314–321.
[26] I.K. Oikonomopoulos, M. Perraki, N. Tougiannidis, T. Perraki, H.U. Kasper, M. Gurk, Clays from Neogene Achlada lignite deposits in florina basin (Western Macedonia, N. Greece): a prospective resource for the ceramics industry, Appl. Clay Sci. 103 (2015) 1–9.
[27] N.M. Musyoka, R. Missengue, M. Kusisakana, L.F. Petrik, Conversion of South African clays into high quality zeolites, Appl. Clay Sci. 97–98 (2014) 182–186.
[28] The International Zeolite Association, S.C., Atlas of Zeolite Framework Types. (www.iza-structure.org/databases/).
[29] D.-C. Lin, X.-W. Xu, F. Zuo, Y.-C. Long, Crystallization of JBW. CAN, SOD and ABW type zeolite from transformation of meta-kaolin, Micropor. Mesopor. Mater. 70 (2004) 63–70.
[30] M. Maldonado, M.D. Oleksiak, S. Chinta, J.D. Rimer, Controlling crystal polymorphism in organic-free synthesis of Na-zeolites, J. Am. Chem. Soc. 135 (2013) 2641–2652.
[31] G. Vassort, J. Whittembury, L.J. Mulins, Increases in internal Ca^{2+} and decreases internal H+ are induced by general anesthetics in squid axons, J. Biophys. Soc. 50 (1986) 11–19.
[32] S.D. Kim, S.H. Noh, J.W. Park, W.J. Kim, Organic-free synthesis of ZSM- 5 with narrow crystal size distribution using two-step temperature process, Micropor. Mesopor. Mater. 92 (2006) 181–188.
[33] S.D. Kim, S.H. Noh, K.H. Seong, W. Jung, Kim. Compositional and kinetic study on the rapid crystallization of ZSM-5 in the absence of organic template under stirring, Micropor. Mesopor. Mater. 72 (2004) 185–192.
[34] I.O. Ali, A.M. Hassan, S.M. Shaaban, K.S. Soliman, Synthesis and characterization of

ZSM-5 zeolite from rice husk ash and their adsorption of Pb^{2+} onto unmodified and surfactant-modified zeolite, Sep. Purif. Technol. 83 (2011) 38–44.
[35] K.S. Suslick, L.A. Crum, M.J. Crocker (Ed.), Encylopedia of Acoustics, John Wiley & Sons, New York, 1997.
[36] K.S. Suslick, Ultrasound: Its Chemical, Physical and Biological Effects, VCH publishers, New York, 1988.
[37] K.S. Suslick, D.A. Hammerton, R.E. Cline, Sonochemical hot spot, J. Am. Chem. Soc. 108 (1986) 5641–5642.
[38] K.S. Suslick, S.J. Doctycz, Interparticle collisions driven by ultrasound, Science 247 (1990) 1067–1069.
[39] S. Shu, S. Husain, W.J. Koros, Sonication-assisted dealumination of zeolite A with thionyl chloride, Ind. Eng. Chem. Res. 46 (2007) 767–772.
[40] J.H. Bang, K.S. Suslick, Applications of ultrasound to the synthesis of nanostructured materials, Adv. Mater. 22 (2010) 1039–1059.
[41] K.S. Suslick, D.A. Hammerton, The site of sonochemical reactions, IEEE Trans. Ultrason. Ferroelect. Freq. Control 2 (1986) 143–147.
[42] C.M. Lousada, M. Yang, K. Nilsson, M. Jonsson, Reactivity of H2O2 towards different UO2-based materials, J. Mol. Catal. A: Chem. 379 (2013) 178–184.
[43] B. Subotic, D. Skrtic, I. Smit, L. Sekovanic, Transformation of zeolite A into hydroxysodalite: I. an approach to the mechanism of transformation and its experimental evaluation, J. Cryst. Growth. 50 (1980) 498–508.
[44] R.I. Walton, F. Millange, D. O'Hare, A.T. Davies, G. Sankar, C.R.A. Catlow, In situ studies of the crystallisation of metal-organic frameworks, J. Phys. Chem. B 105 (2001) 83–90.
[45] B. Bayati, A.A. Babaluo, P. Ahmadian Namini, Synthesis and seeding time effect on the performance of nanostructure sodalite membranes, IJChE 4 (2007) 54–70.
[46] W. Franus, M. Wdowin, M. Franus, Synthesis and characterization of zeolites prepared from industrial fly ash, Environ. Monit. Assess. 186 (2014) 5721–5729.
[47] J. Park, B.C. Kim, S.S. Park, H.C. Park, Conventional versus ultrasonic synthesis of zeolite 4A from kaolin, J Mater Sci Lett. 20 (2001) 531–533.
[48] L. Itani, Y. Liu, W. Zhang, K.N. Bozhilov, L. Delmotte, V. Valtchev, Investigation of the physicochemical changes preceding zeolite nucleation in a sodium-rich aluminosilicate gel, J. Am. Chem. Soc. 131 (2009) 10127–10139.
[49] K.S. Suslick, S.J. Doktycz, The effects of ultrasound on solids, in: T.J. Mason (Ed.), Advances in Sonochemistry, JAI Press, New York, 1990, pp. 197–230.
[50] D.P. Serrano, R.V. Grieken, Heterogeneous events in the crystallization of zeolites, J. Mater. Chem. 11 (2001) 2391–2407.
[51] C. Quintelas, H. Figueiredo, T. Tavares, The effect of clay treatment on remediation of diethylketone contaminated wastewater: uptake, equilibrium and kinetic studies, J. Hazard. Mater. 186 (2011) 1241–1248.
[52] Z. Huo, X. Xu, Z. Lv, J. Song, M. He, Z. Li, Q. Wang, L. Yan, Y. Li, Thermal study of NaP zeolite with different morphologies, J. Therm. Anal. Calorim. 111 (2013) 365–369.
[53] A. Demortier, N. Gobeltz, J.P. Lelieur, C. Duhayon, Infrared evidence for the formation of an intermediate compound during the synthesis of zeolite Na–A from metakaolin, Int. J. Inorg. Mater. 1 (1999) 129–134.
[54] G.G. Fuentes, A.R. Ruiz-Salvador, M. Mir, O. Picazo, G. Quintana, M. Delgado, Thermal and cation influence on IR vibrations of modified natural clinoptilolite, Micropor. Mesopor. Mater. 20 (1998) 269–281.
[55] C.A. Ríos, C.D. Williams, M.J. Maple, Synthesis of zeolites and zeotypes by hydrothermal transformation of kaolinite and metakaolinite, BISTUA 5 (2007) 15–26.
[56] B.R. Albert, A.K. Cheetham, J.A. Stuart, C.J. Adams, Investigations on P zeolites: synthesis, characterization, and structure of highly crystalline low-silica NaP, Micropor. Mesopor. Mater. 21 (1998) 133–142.
[57] V.L. Zholobenko, J. Dwyer, R. Zhang, A.P. Chapple, N.P. Rhodes, J.A. Stuart, Structural transitions in zeolite P: an in situ FTIR study, J. Chem. Soc. Faraday Trans. 94 (1998) 1779–1781.
[58] E.M. Flanigen, Advances in Chemistry. A Review and New Perspectives in Zeolite Crystallization, second ed., American Chemical Society, Washington, 1973, pp. 119–139.
[59] Y.K. Kim, K.P. Rajesh, J.-S. Yu, Zeolite materials prepared using silicate waste from template synthesis of ordered mesoporous carbon, J. Hazard. Mater. 260 (2013) 350–357.
[60] K. Aoki, K. Kusakabe, S. Morooka, Gas permeation properties of A-type zeolite membrane formed on porous substrate by hydrothermal synthesis, J. Membr. Sci. 141 (1998) 197–205.
[61] A. Huang, N. Wang, J. Caro, Stepwise synthesis of sandwich-structured composite zeolite membranes with enhanced separation selectivity, Chem. Commun. 48 (2012) 3542–3544.
[62] A. Huang, J. Caro, Cationic polymer used to capture zeolite precursor particles for the facile synthesis of oriented zeolite LTA molecular sieve membrane, Chem Mater. 22 (2010) 4353–4355.